A pumpless unidirectional perfusion system for Vessel-on-Chip models utilising Tesla Valves

Bo Stok
Biomedical Technology (BMT), Bachelor thesis
Applied Microfluidics for BioEngineering Research (AMBER) group
University of Twente, Faculty Electrical Engineering, Mathematics and Computer Science (EEMCS),
Enschede, The Netherlands
Student number: s2854007, Email: b.stok@student.utwente.nl
Committee:
prof.dr.ir. Séverine Le Gac (chair) - Guillaume Coindreau (daily supervisor) - prof.dr.ir Mathieu Odijk (extern)

July 7, 2025

Abstract

This study presents the development of a pumpless unidirectional perfusion system utilising Tesla Valves (TV's) combined with a rocking platform to model physiological blood flow within a Vessel-on-Chip (VOC) model. Overcoming limitations related to traditional pump and pumpless based perfusion methods, the system utilises TV's to achieve flow through the VOC without moving parts, improving simplicity, cost efficiency, and miniaturisation. Multiple TV designs were characterised by measuring flow rates at specific applied pressure drops, evaluating the most effective design based on diodicity. The optimised TV was combined into a VOC model, resulting in a system consisting of two reservoirs connected by a VOC channel and a TV channel. The system is modelled with the hydraulic electrical analogy to estimate backflow and Wall Shear Stress (WSS) on the VOC. The calculations demonstrate that while the system generates the required pressure drop and WSS to model liver sinusoidal endothelial cells, it presents considerable backflow, preventing unidirectional flow. Consequently, the system is unsuitable for organ-on-chip (OOC) models requiring unidirectional flows. Future improvements should focus on reducing backflow, potentially through improving the geometry of the TV or implementing additional TV's in the VOC channel. This research establishes a foundation for utilising TV pumpless perfusion systems with potential advantages in miniaturisation and operational simplicity, contributing to the advancement of microfluidic organ models.

Deze studie beschrijft de ontwikkeling van een pomploos unidirectioneel perfusie systeem waarbij Tesla kleppen (TV's) worden gecombineerd met een kantelplatform om de fysiologische bloedstroom binnen een Vessel-On-Chip (VOC) model na te bootsen. Om beperkingen van traditionele pomp- en pomploze perfusiemethoden te overwinnen, maakt het systeem gebruik van TV's om stroming door de VOC te realiseren. Deze methode geeft geen bewegende delen, wat resulteert in een operationele eenvoud, kosten efficiëntie en miniaturisatie. Meerdere TV ontwerpen werden gekarakteriseerd door het meten van debieten bij specifieke drukverschillen, waarbij het meest effectieve ontwerp werd geselecteerd op basis van diodiciteit. De geoptimaliseerde TV werd geïntegreerd in het VOC model, wat resulteerde in een systeem bestaande uit twee reservoirs die verbonden zijn via een VOC kanaal en een TV kanaal. Het systeem werd gemodelleerd met behulp van de hydraulisch-elektrische analogie om terugstroom en wand schuifspanning (WSS) in de VOC te berekenen. Deze berekeningen tonen aan dat het systeem de vereiste drukval en WSS kan genereren om lever sinusoïdale endotheelcellen te modelleren, maar het systeem genereerd ook een aanzienlijke terugstroom, waardoor er geen unidirectionele stroming kan plaatsvinden. Hierdoor is het systeem ongeschikt voor Organ-On-Chip (OOC) modellen die unidirectionele stromingen vereisen. Toekomstige verbeteringen zouden zich moeten richten op het verminderen van terugstroom in de VOC, mogelijk door het optimaliseren van de geometrie van de TV of door het implementeren van extra TV's in het VOC kanaal. Dit onderzoek legt een basis voor het gebruik van pomploze perfusie systemen met TV's, met potentiële voordelen op het gebied van miniaturisatie en operationele eenvoud, en draagt bij aan de ontwikkeling van microfluïdische orgaanmodellen.

Introduction

Organ-On-Chip (OOC) models show great promise in modeling the function of human organs and tissue *in vitro* [1]. These models combine microfluidics and cell biology and can serve multiple purposes. One of these is to gain a deeper understanding of the physiological processes in the human body and of diseases [2]. For example, OOC models can be used to study the formation of cancer metastasis, allowing the development of anti-metastasis treatment [3]. Another application of OOC models is in the pharmaceutical industry, and particularly in drug development and testing. Furthermore, OOC models can serve as an alternative to animal testing due to a more accu-

rate representation of the human physiology versus animals [4, 5].

An important factor to consider in OOC models is perfusion as for instance within blood vessels to provide nutrition to the cells [6]. *In vivo*, perfusion is continuous and unidirectional through a blood vessel and creates a Wall Shear Stress (WSS) on the endothelial cells. The WSS is crucial for the controlled permeability of the blood vessel, the morphology and function of the endothelial cells. An accurate representation of the physiological WSS within the OOC model is crucial as the WSS is optimized for each tissue/organ [7, 8, 9].

Existing techniques for achieving constant unidirectional perfusion rely on pressure controlled pump-based systems (peristaltic or syringe pumps) [10]. However, these setups require external tubing and demand a large space. To overcome these limitations, pumpless systems that mostly utilise gravity-driven flow have been developed [11]. Unfortunately, these systems require frequent manual refills, which increases the labour intensity for long-term experiments [11]. As an alternative, pumpless strategies based on rocking platforms have been developed. The rocking platform generates a flow through the channel by using the height difference between two reservoirs [12]. A limitation for these systems is that they are mostly not unidirectional, and tend to be bulky, as they are not simple PDMS-glass devices, which may be preferable in certain applications such as cell imaging [13].

A potential solution to reduce these limitations is the use of a Tesla Valve (TV) in combination with a rocking platform. A TV is a passive valve that contains no moving parts, making it cost-efficient, ideal for compact systems and easy to fabricate [14]. Its asymmetric geometry allows the fluid in a TV to easily flow in one direction (forward flow), while simultaneously restricting flow in the opposite direction (reverse flow), as shown in Figure 1. The functionality of TV's has been tested at microfluidic scale, and utilised within sweat collection devices to prevent backflow [15, 16]. However, their use in OOC research remains limited.

This study describes the development of a pumpless unidirectional perfusion system, utilising a combination of TV's and a rocking platform. Their diodicity is to be evaluated through the determination of the flow rate through the TV at various pressure drops in both a reverse and forward flow configuration. Subsequently, the most promising design is to be embedded in a Vessel-On-Chip (VOC) model to analyse the possible backflow during forward flow through the hydraulic-electrical analogy. This analogy describes the connection between a hydraulic system and an electric circuit, resulting in the ability to model fluidic behaviour using electrical components. Lastly, the hydraulic-electrical analogy is to be applied to evaluate whether the system can model liver sinusoid endothelia, where the WSS ranges from 0.1 to 0.5 dyn/cm^2 [18, 19].

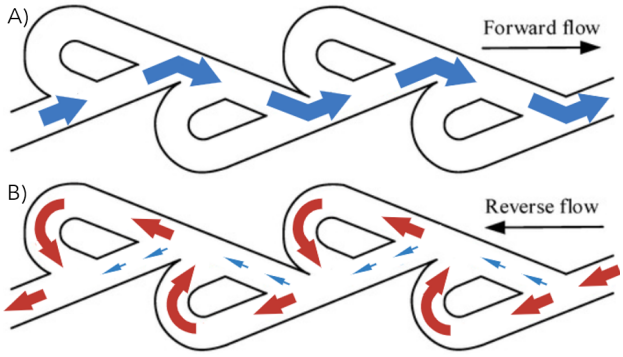

Figure 1: *The principle of Tesla valves: during forward flow (A), the fluid moves easily through the main channel, whereas in reverse flow (B) it becomes restricted, as the fluid is directed through the side loops. This figure is based on [17] and has been adapted using www.BioRender.com.*

Technical framework

Tesla Valve

The performance of a TV can be determined by calculating the diodicity (*Di*), where the *Di* is the ratio between the forward flow rate (Q_f) and the reverse flow rate (Q_r) measured at the same applied pressure drop (ΔP):

$$Di = \left(\frac{Q_f}{Q_r}\right)_{\Delta P} \tag{1}$$

A TV is considered to work when $Di > 1$, indicating that the TV provides greater resistance in the reverse direction, as shown by a lower Q_r. In other words the reverse hydraulic resistance (R_r) is higher than the forward hydraulic resistance (R_f). While a higher *Di* means a more effective TV, therefore, it is desirable to design a TV with the highest possible *Di* [20, 21]. A *Di* higher then 2 is preferred for practical applications [22]. Unfortunately, due to the small scale and the low flow rate in OOC models, the *Di* is estimated to be between 1 and 2 depending on the TV design [23].

The geometry of a TV has a significant impact on the *Di* [24]. A schematic representation of a TV is shown in Figure 2. Here, the TV's parameters are defined as, w (the width of the loop, in mm), d (the width of the main channel in the loop, in mm), r_{loop} (the radius of the loop, in mm), x (the width of the main channel outside the loop, 0.5 mm), H (the height of the channel and loop, 0.5 mm), α (the angle

of the loop, 60 °) and n (the number of loops, 3). In this study, parameters w, d and r_{loop} are varied to optimise the TV's Di. Table 1 summarises the values of the altered parameters and their expected impact on the Di in comparison with design 1 [24, 25, 26]. Each design was based on TV design 1 (w = 0.5 mm, d = 0.5 mm and r = 1.25 mm), which is inspired by existing literature and scaled down accordingly (Figure 2A) [16, 26, 27], with the exception of design 2, which is based of a GMF TV model (Figure 2B). The main difference between these models is the shape of the loop, with the return angle at the end of the loop being larger in the GMF model (Figure 2). This TV model has been chosen as a parameter due to its promising results in previous studies [25, 26]. The values of the parameters corresponds to those specified in their SOLIDWORKS 2024 design.

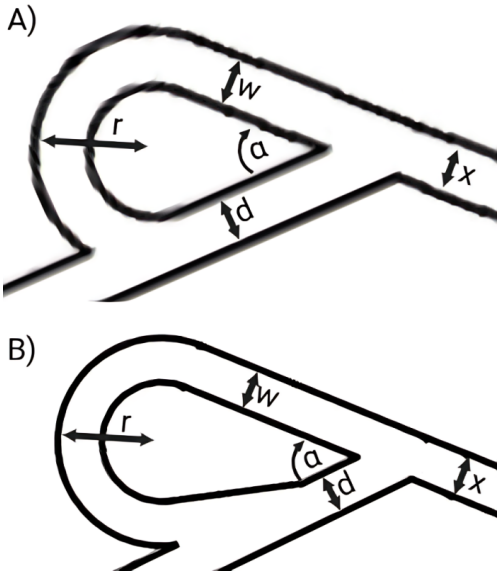

Figure 2: *A schematic visualisation of the parameters of the loop in the Tesla Valve designs. A) The TV design used for designs 1, 3 and 4. B) The GMF Tesla Valve design used for design 2. With w the width of the loop, d the width of the main channel in the loop, r the radius of the loop, α the angle of the loop and x the width of the main channels outside the loops. This figure is based on [26], and adapted using www.Biorender.com.*

Table 1: *Values of the varied parameters for each TV design tested in this study, and their impact on Di in comparison with design 1.*

Design	w (mm)	d (mm)	r_{loop} (mm)	*Di*
1	0.5	0.5	1.25	–
2	0.62	0.5	1.05	↑
3	0.5	0.3	1.25	↑
4	0.75	0.5	1.25	↑

In addition to the geometry, the Reynolds number (Re) of the flow also impacts the Di of the TV. The Re predicts the behavior of a flow. When $Re > 4000$, the flow is turbulent, characterised by chaotic and unpredictable movement. For $Re < 2000$, the flow is laminar, meaning that the fluid travels in parallel layers without mixing. When $Re \ll 1$, there is a so-called creeping flow, resulting in a flow where viscous forces dominate inertial forces. In OOC models, the Re is typically low due to its small scale and low flow rates, resulting in a laminar of even creeping flow. Several studies show that Di tends to decrease with decreasing Re, (Di of 1.05 at Re of 100, and Di of 1.1 at Re of 150 [28, 29]). Although TV's can still operate at a low Re, it is important that Re does not drop significantly below 1. If this occurs, creeping flow conditions (viscous forces) dominate, resulting in a Di going to 1, meaning that the effectiveness of a TV significantly reduces [23].

Re can be estimated as follows:

$$Re = \frac{D_h \cdot v \cdot \rho}{\mu} \tag{2}$$

Where: D_h is the hydraulic diameter of the channel (in m), ρ is the fluid density (in kg/m^3), v is the flow velocity (in m/s) and μ is the dynamic fluid viscosity (in Pa· s).

Rocking platform

A rocking platform is a mechanical device that alternatively raises and lowers the opposite sides of a flat surface. When a system, existing of two fluid reservoirs connected with a channel, is put on a rocking platform, the fluid level in one reservoir becomes higher than the other one. This height difference (Δh) results in a hydrostatic pressure difference (ΔP_h) between the fluids in the reservoirs. According to the hydrostatic principle, the fluid flows from the reservoir with the higher fluid level to the lower one until equilibrium is reached. The hydrostatic pressure can be expressed as:

$$\Delta P_h = \Delta h \cdot \rho \cdot g \tag{3}$$

Where: ρ is the density of the fluid (in kg/m^3) and g is the gravitational acceleration (9.81 m/s^2).

As mentioned before, when to accurately model physiological conditions, it is important to maintain a constant WSS within a specific range. However, Equation 3 shows that decreasing Δh, results in a decreasing ΔP_h, which in turn decreases the flow rate and consequently the WSS in the VOC. This may result in a WSS that falls outside the desired range. To prevent this, the tilting duration and tilting angle of the rocking platform can be adjusted accordingly. By combining equation 3 with the distance between the reservoirs (l, in m), the angle of the rocking platform can be determined for certain pressure drops.

The angle of the rocking plate can be expressed as:

$$\beta = sin^{-1}\left(\frac{\Delta P}{l \cdot \rho \cdot g}\right) \quad (4)$$

Full system

The full concept for the proposed pumpless perfusion system involves two reservoirs, connected by two channels. One channel contains the VOC model, with a height and width of both 0.25 mm and a length of 5.5 mm. The other channel contains 3 TV's. The system and all its components are illustrated and defined in Figure 3. If the system is placed on a rocking platform without any tilt, no flow occurs, as shown in Figure 4A. However, when the platform tilts to generate reverse flow, the principle of the TV's should ensure that R_r is higher than that of the VOC. This causes the fluid to flow through the VOC channel, as illustrated in Figure 4B. On the other hand, during forward flow, if R_f is lower than that of the VOC, the fluid mainly flows through the TV channel, as shown in Figure 4C. This overall working principle is shown in Figure 4.

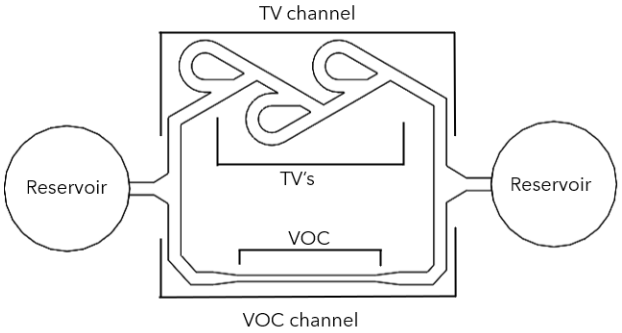

Figure 3: *A schematic representation of the system, illustrating the reservoirs, TV's, TV channel, VOC, and VOC channel.*

It is important to mention that not all the fluid exclusively goes through the TV channel during the forward flow. Some fluid still flows through the VOC channel, resulting in a backflow. Minimising the duration of the backflow is crucial to reduce the time during which the cells are exposed to WSS in the opposite direction. This can be achieved by rapidly tilting the rocking platform to the maximum tilt angle, at which the channels remain filled with fluid.

Using the hydraulic–electrical analogy, the full system can be modelled as an electric circuit (Figure 5), where the hydraulic resistances (R_h) of the channels correspond to electrical resistances (R_e), the pressure drop (ΔP) to a voltage (V) and the flow rate (Q) to a current (I). Knowing this relation between these parameters, the fluid version of Ohm's law can be used:

$$\Delta P = R_h \cdot Q \quad (5)$$

Were: ΔP is the pressure drop (Pa), Q is the flow rate (m^3/s) and R_h is the hydraulic resistance ($Pa{\cdot}s/m^3$).

By expressing the full system as an electric circuit, series and parallel principles can be used in combination with the fluid version of Ohm's law (Equation 5) to calculate unknown parameters for different parts of the full system. For instance, the pressure drop over the whole system (ΔP_{tot}), to maintain a WSS of 0.1-0.5 dyn/cm^2 on the VOC, can be calculated. The same principles apply for the backflow in the VOC during forward flow.

However, to be able to calculate these parameters, the hydraulic resistances of the different parts of the full system must be calculated. This can be done using the Hagen-Poiseuille Equation 6-8. Equation 6 is used for channels with a rectangular cross section, Equation 7 is used for channels with a square cross section (H = W), and Equation 8 for channels with a circular cross section.

$$R_{h,rectangular} = \frac{12 \cdot \mu \cdot L}{1 - 0.63 \cdot (\frac{H}{W})} \cdot \frac{1}{H^3 \cdot W} \quad (6)$$

$$R_{h,square} = \frac{12 \cdot \mu \cdot L}{1 - 0.917 \cdot 0.63} \cdot \frac{1}{H^4} \quad (7)$$

$$R_{h,circular} = \frac{8 \cdot \mu \cdot L}{\pi \cdot R^4} \quad (8)$$

Were: H is the height of the channel (m), W is the width of the channel (m), L is the length of the channel (m), μ is the dynamic fluid viscosity ($Pa{\cdot}$ s) and R is the radius of the channel (m).

Methods

Mould fabrication

The TV moulds were designed using SOLIDWORKS 2024 and subsequently fabricated via stereolithography (SLA) using a Form 3B+ printer (Formlabs) and Clear v4 resin. After printing, the moulds underwent a series of post-processing steps, based on a study of Venzac et al. [30]. In the first step, the moulds were cleaned with isopropanol (IPA, Sigma Aldrich) and placed in a sonicator (Formlabs) filled with IPA for one hour. For the second step, the moulds were transferred to an UV Curer (Formlabs, 253.7 nm) for 1 hour at 45 °C. Finally, the moulds were placed in a dry oven (Binder) overnight at 65 °C.

Tesla Valve chip fabrication

To fabricate the full TV chips, a 10:1 (w:w) mixture of PDMS base and curing agent (SYLGARD 184 Silicone

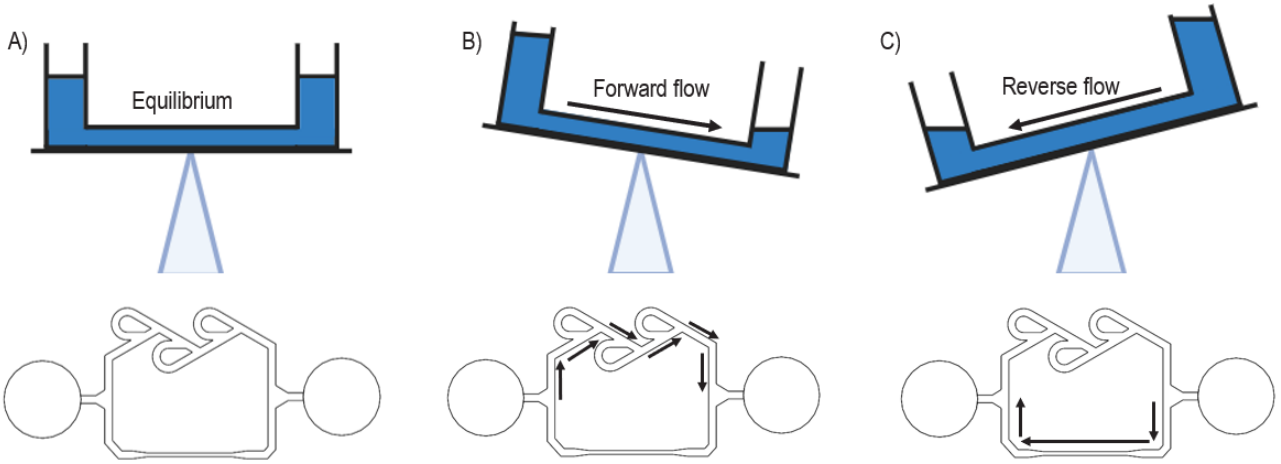

Figure 4: *The principle of the pumpless unidirectional perfusion system utilising a combination of TV's and a rocking platform. A) The system is at a equilibrium, the fluid levels in both reservoirs are equal and no flow is present. B) The fluid level in the left reservoir is higher, resulting in a forward flow mainly through the TV channel. C) The fluid level in the right reservoir is higher, resulting in a reverse flow mainly through the VOC channel. This figure is made using www.BioRender.com.*

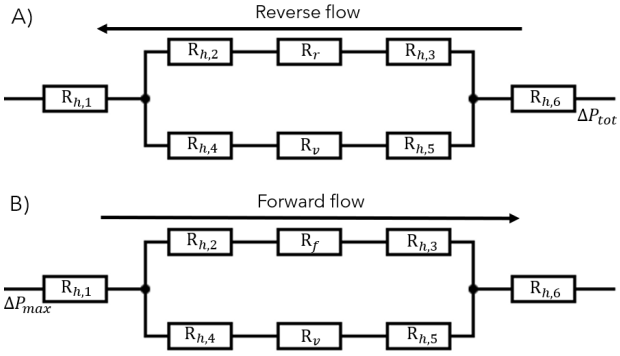

Figure 5: *The hydraulic-electric analogy of the full system, A) The electric circuit during reverse flow. B) The electric circuit during forward flow. This figure is designed using www.CircuitDiagram.com.*

Elastomer Kit) was prepared. The PDMS mixture was poured into the TV moulds and degassed in a vacuum chamber for 30 minutes. Subsequently, the filled TV moulds were cured overnight in an oven (Binder) at 65 °C. The PDMS TV chips were then removed from the moulds and circular holes, 1.2 mm diameter, were punctured at the inlet and outlet. Following the puncturing, the PDMS TV chip and a glass slide were placed in a plasma cleaner (henniker plasma, HPT-200) to activate their surfaces. The activated surface of the PDMS TV chip was pushed against the activated surface of the glass slide, resulting in bonding between the PDMS TV chip and the glass slide.

Characterisation of the Tesla Valves

Prior to each test, the full TV chip (consisting of the bonded PDMS TV chip and glass slide) was exposed to a second plasma treatment in a plasma cleaner (henniker plasma, HPT-200), this time to make the channels hydrophilic rather than for bonding purposes. Subsequently, the full TV chip was connected to enable reverse flow through the TV's, using: (i) two Push Pull controllers (Fluigent) to regulate the pressure difference in the setup, (ii) two fluid reservoirs, and (iii) one FLOW UNIT M sensor (Fluigent) to measure the flow rate through the setup.

Once the setup was assembled, any air bubbles present within the TV's were manually removed by gently pressing on the chip to expel them. A pressure difference of 0.6 mbar was then applied across the setup to establish a baseline flow rate of 0.0 $\pm$ 0.2 μ l/min (as a base line), as measured by the flow sensor. The flow rate was then measured for increasing pressure difference steps of 0.6 mbar, occasionally increasing to 0.7 mbar due to fluctuations within the setup, with a minimum of 16 steps. Subsequently, the full TV chip was reconnected to establish a forward flow, and the same procedure was repeated. Each TV design was tested in triplicate (n = 3). The liquid used for the tests was deionised water at 20 ° C.

Data processing

To be able to process the data, the exact ΔP across the TV's was determined for each test. This was achieved by expressing the measuring setup into an electric circuit, using the hydraulic-electrical analogy (Figure 6B). Afterwards, Equation 8 was used to calculate $R_{tube,1}$, $R_{tube,2}$, $R_{metal,1}$, $R_{metal,2}$ and R_{sensor}. Using these resistances in combination with the series principle and Equation 5, ΔP across the TV's was calculated for each test. The mean Di for each TV design was calculated using Equation 1 for each specific ΔP

and plotted as a diagram against the corresponding ΔP .

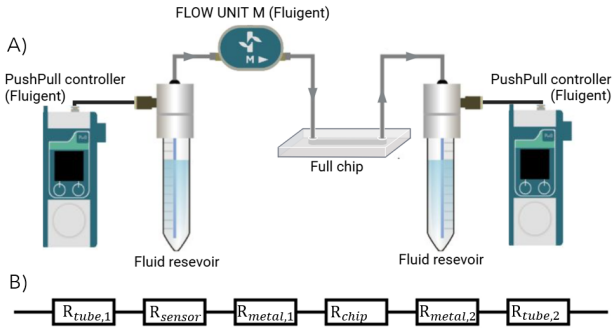

Figure 6: *The Fluigent setup used to characterise the Telsa Valves. A) A schematic visualisation of the used Fuigent setup, to measure the flow rate through the Tesla Valve at the applied pressure drops. B) The electric circuit of the used Fluigent setup. These figures are made with www.Biorender.com and www.CircuitDiagram.com, based on [31].*

Based on the resulting *Di* diagram, the TV design with the highest *Di* at the desired pressure drop was selected, and its R_r and R_f values were calculated. To calculate the R_r the reverse flow data were used, and for R_f the forward flow data. The R_r and R_f values were calculated using Equation 5 in combination with the measured Q and the corresponding ΔP, and plotted against the corresponding ΔP. Subsequently, the plotted values of R_r were used to estimate the R_r at the desired pressure drop, which in turn allowed for the calculation of the total pressure drop (ΔP_{tot}) required to generate a wall shear stress range of 0.1-0.5 dyn/cm^2 in the VOC. ΔP_{tot} was then used in Equation 3 to determine if ΔP could be achieved using a rocking platform. Additionally, the R_f was estimated at the maximum pressure drop of the full system to calculate the WSS and duration of the backflow.

Dimensions of the VOC and TV design

The VOC PDMS chip and the TV design corresponding to the highest *Di* at the desired pressure drop were fabricated according to the procedure of the TV chip fabrication section, excluding the bonding to the glass slide. The dimensions of these PDMS chips were subsequently measured using the VK-X3000 microscope (Keyence). For both the VOC and the TV design, the measurements were performed in triplicate. The obtained data were analysed using the VK-X3000 MultiFileAnalyzer software, and the average values for the dimensions were calculated.

Results and Discussion

PDMS VOC chip dimensions

The dimensions of the VOC were measured according to the procedure mentioned in 'Dimensions of the VOC and TV design and were obtained as 0.26 mm (W), 0.24 mm (H) and 5.5 mm (L). These values match closely to the dimensions that were specified in SOLDWORKS 2024, with only minor differences, the H is 0.01 mm smaller and the W is 0.01 mm larger. These minor differences are unlikely to have a significant impact on the hydraulic performance of the system, however, these measured dimensions are used for the future calculations to ensure accuracy.

Pressure drop in the VOC channel

Using the dimensions of the VOC obtained in the PDMS VOC chip dimensions section, the theoretical R_h of the VOC (R_v) was calculated using Equation 6, resulting in a value of $4.39{\cdot}10^{10}$ Pa$\cdot$ s/m^3. The data obtained using the method provided in appendix A, show an average R_v of $4.12{\cdot}10^{11} \pm 6.76{\cdot}10^{10}$ Pa$\cdot$ s/m^3. This large difference could be explained by the possible imperfections in the ridges of the casted PDMS VOC, as well as the fact that the measurements were obtained using the method in Appendix A and not the method described in the Characterisation of the TV section, leading to a possible higher standard deviation. That said, the measured R_v reflects realistic conditions better and therefore will be used in this study. Based on this R_v, the total R_h across the VOC channel ($R_{v,tot}$) was calculated using Equation 7 and the principle of resistances in series, by summing $R_{h,4}$, $R_{h,5}$ and R_v (Figure 5). This results in a $R_{v,tot}$ of $4.19{\cdot}10^{11}$ Pa$\cdot$s/m^3. Subsequently, $R_{v,tot}$ was used in combination with Equation 5 to calculate the pressure drop across the VOC channel for a WSS of 0.1 and 0.5 dyn/cm^2 in the VOC. For a WSS of 0.1 dyn/cm^2, the pressure drop was 10.91 Pa, and for 0.5 dyn/cm^2, it was 54.51 Pa. Due to the fact that the TV channel runs in parallel to the VOC channel (see Figure 5), these pressure drops are also present across the TV channel.

Di analysis

The calculated *Di* from the three tested designs is presented in Figure 7. The results indicate a general trend in which the *Di* increases at lower pressure differences (low flow rate and low *Re*). This observation does not align with the other findings in previous studies [26, 28, 29]. A likely explanation is related to the limitations of the setup. The FLOW UNIT M (Fluigent) has an accuracy of 0.12 μl/min for flow rates below 2.4 μl/min [32], which means that the

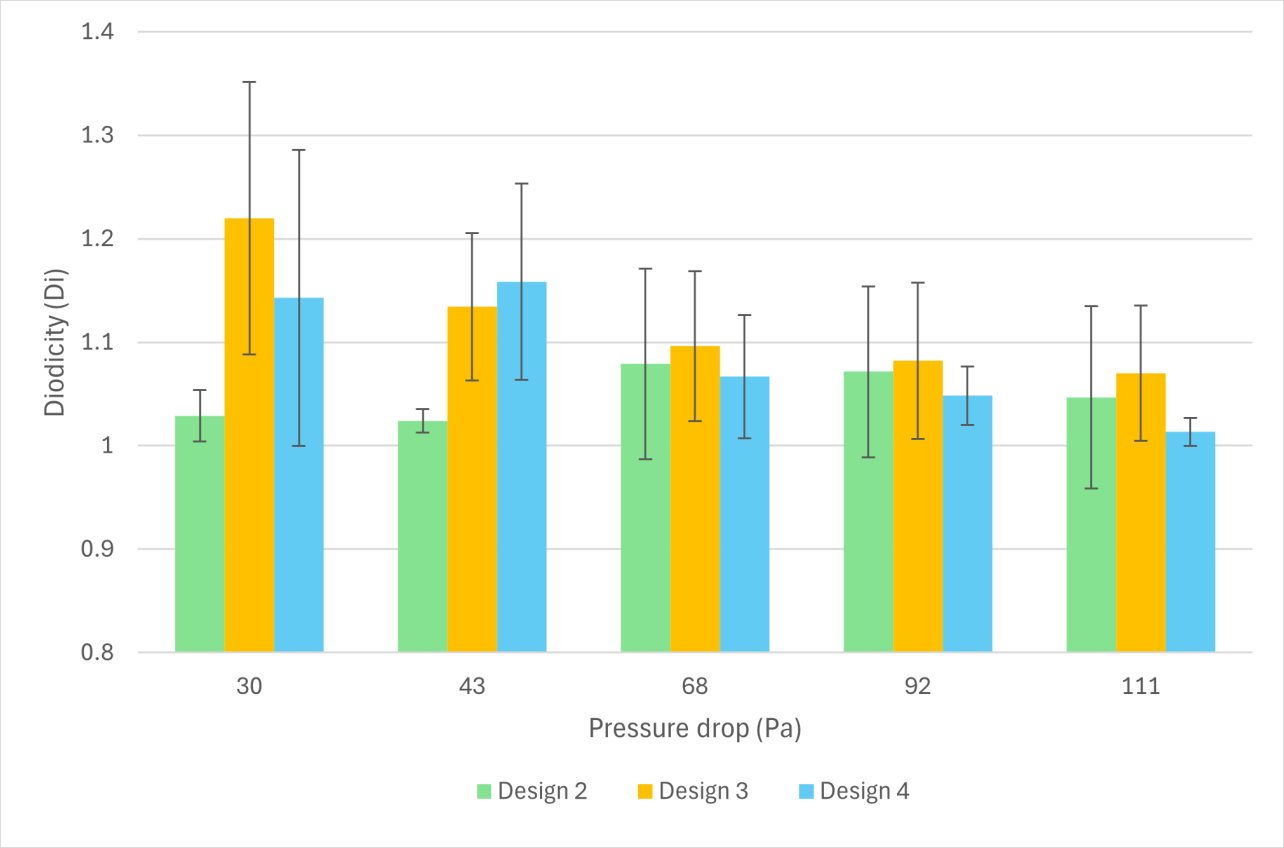

Figure 7: *The diodicity of the TV designs 2, 3 and 4 plotted against the pressure drop. n = 3 and the error bars are shown as standard deviation.*

desired low flow rate could not be measured reliably using the current setup.

Design 3 (smaller d) has a higher Di than design 2 at the desired pressure drop (11 to 55 Pa). This can be seen as that the lowest Di value of design 3, within the standard deviation, is still higher than the highest value Di of design 2 within its standard deviation, respectively 1.22 ± 0.14 vs 1.02 ± 0.02. In contrast, comparing designs 3 and 4 at the same pressure drop range is more difficult. Even though, the mean Di of design 4 is higher at the higher range of the pressure drop (55 Pa), design 3 has a higher mean Di at the lower end. Furthermore, Figure 7 shows that the standard deviation for both designs overlaps, which means that the difference may not be statistically significant. As a consequence of the slightly lower standard deviation and the higher Di over the majority of the pressure drop range between 11 and 55 Pa, design 3 was selected for the full system. It should be mentioned that design 4 was tested one day prior to designs 3 and 2. This meant that the tests were not carried out under the same conditions. As a result, the flow sensor was cleaned to avoid clogging that could occur if residual fluid dry out overnight. This cleaning step may have impacted the consistency of results. If there was a clog beforehand, removing it could have changed the conditions. For future research, it should be kept in mind that the measurements should all be conducted under the same conditions. Additionally, to make sure to have accuracy at low flow rates, a more suitable sensor should be used. The FLOW UNIT S sensor (Fluigent) is recommended for future studies at these low flow rates, as it is more accurate and should reduce the variation in the measured values.

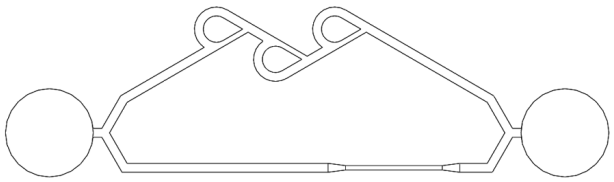

Figure 8: *The full system design including the integration of TV design 3.*

PDMS TV chip dimensions

The measured dimensions of TV design 3 were obtained as 0.51 mm (w), 0.32 mm (d), 1.27 mm (r), 0.50 mm (H) and 0.51 mm (x). The dimensions specified in the SOLIDWORKS 2024 design are shown in Table 1. These dimensions have minor differences, w is 0.01

mm larger, d is 0.02 mm larger, r is 0.02 mm larger and x is 0.01 mm larger. These minor differences are unlikely to have a significant impact on the hydraulic performance of the system, however, these measured dimensions are used for the future calculations to ensure accuracy.

R_r, R_f and Re analysis

As mentioned before in the Data processing section, R_r and R_f were calculated for each applied pressure drop. The results are shown in Figure 9. Overall, both resistances stay fairly stable, with exception of the first two values. The first values of R_r and R_f show the highest resistances, while the second values show the lowest resistances. Due to the significant differences between these two values and the stability of the other values, it was decided to use the average value of R_r and R_f for further calculations.

The average value of R_r was found to be $5.83{\cdot}10^{11}$ $\pm$ 6.15 $\cdot 10^{10}$ Pa$\cdot$ s/m^3 and that of R_f was $4.62{\cdot}10^{11}$ $\pm$ 3.99 $\cdot 10^{10}$ Pa$\cdot$ s/m^3. Using the measured R_r, the ΔP_{tot} required to achieve a WSS value of 0.1 and 0.5 dyn/cm^2 was calculated. For a WSS of 0.1 dyn/cm^2, ΔP_{tot} was 10.93 Pa and for a WSS of 0.5 dyn/cm^2, it was 54.74 Pa. Using these values in combination with Equation 3, Δh was calculated for both cases, $\Delta h_{0.1}$ = 1.1 mm and $\Delta h_{0.5}$ = 5.6 mm. Comparing this to the Δh_{max} (6 mm), it indicates that the developed pumpless perfusion system can be used to model the WSS in a liver sinusoid.

R_r can also be used to estimate Re of the flow through the TV's. To do so, first the flow rate through the TV's must be calculated. Using Equation 5, the average R_r and ΔP as 10.91 and 54.51 Pa. The resulting flow rates were $1.85{\cdot}10^{-11}$ m^3/s and $9.28{\cdot}10^{-11}$ m^3/s respectively. Using these flow rates and the measured cross sectional area of the TV inlet, the average velocity (v) was calculated and subsequently used to calculate the Re. The calculated Re values were 0.037 for 10.91 Pa and 0.18 for 54.51 Pa. Both are significantly below 1, indicating that the creeping flow dominates. Meaning the Di should be tending to 1. However, as shown in Figure 7, the Di of TV design 3 is estimated as 1.11 $\pm$ 0.07 at a pressure drop of around 54 Pa. The Di is even higher at a lower pressure drop of 30 Pa. However, it is difficult to estimate Di at pressure drops lower than 30 Pa, due to the limited data. Still, this outcome is unexpected. A likely explanation is that the used flow rate sensor lacked accuracy at these low flow rates and that the setup could not provide a precise pressure drop. As mentioned before, it is important that equipment suited for measuring at lower flow rate and pressure should be used.

Backflow analysis

As mentioned in the introduction, minimising the duration of the backflow is important to limit the time during which the cells are not perfused. This is achieved by rapidly tilting the rocking platform to the maximum tilt angle, at which the channels remains filled with fluid (βmax). βmax was calculated by using Equations 3 and 4, where Δh equals the height of the reservoirs (3 mm) and l the distance between the reservoirs (24.35 mm). This result in a βmax of 7.08 $^\circ$.

When the left reservoir is fully filled (Δh = 6 mm) and the rocking platform tilted to this maximum angle, the maximum pressure drop (ΔP_{max}) across the system is 57.5 Pa. Assuming this pressure remains constant, the resulting backflow generates a WSS of 0.53 dyn/cm^2 for a duration of 224 s. In practice, however, ΔP decreases as Δh reduces, which leads to a decreasing flow rate over time. As a result, the duration of the backflow increases, while the WSS decreases. Ideally, both the duration of backflow and the magnitude of the WSS should be minimised. Based on these findings, the full system does not provide an unidirectional perfusion. As a result, the system is not suitable to use for OOC models that require unidirectional flow.

However, a possible solution to reduce the duration of the backflow is to optimise the geometry of the TV in a way to decrease R_f, allowing more fluid to pass through the TV channel. A possible optimisation could be to increase w of the TV. However, it is important that this improvement does not significantly reduce R_r.

A different solution that can be used to reduce the WSS of the backflow is to add one or multiple TV's to the VOC channel, oriented in the opposite direction to the TV's in the TV channel. The added TV's increases the $R_{v,tot}$ during forward flow, resulting in a reduced WSS. The $R_{v,tot}$ also increases during the reverse flow, resulting in a increase in pressure drop through the system to get the desired WSS on the VOC. However this is significant smaller than the $R_{v,tot}$ during forward flow.

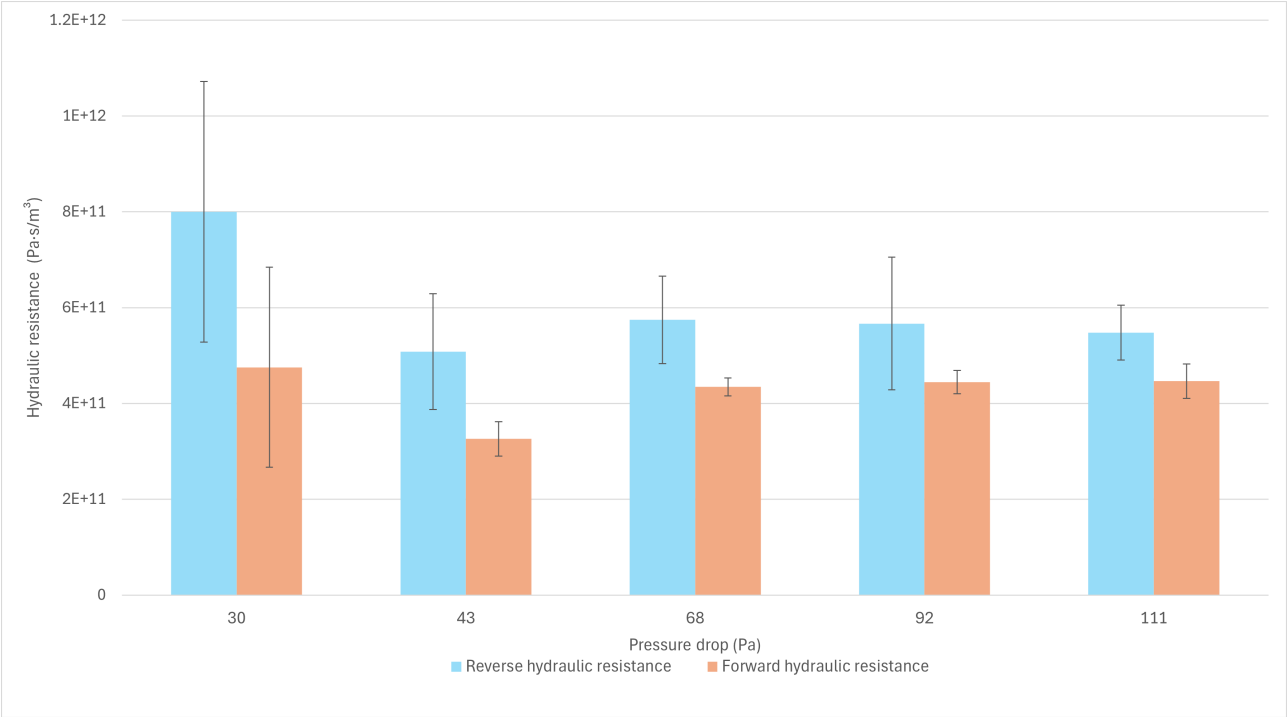

Figure 9: *Reverse hydraulic resistance (R_r) and forward hydraulic resistance (R_f) of Tesla Valve design 3 plotted against the pressure drop. n = 3 and the error bars are shown as standard deviation.*

Conclusion

The developed pumpless perfusion system is capable of generating the required pressure drop, and consequently the WSS, to model liver sinusoidal endothelial cells *in vitro*. However, due to the considerable backflow through the VOC, the system fails to provide unidirectional flow. Therefore, it cannot be adopted as a pumpless unidirectional perfusion system for OOC models. Future research should aim to minimise both the duration and WSS of the backflow, for example by optimising the TV design or incorporating a TV to the VOC channel. Nevertheless, it should be noted that a certain degree of backflow is inherent to the use of TV's within the system. Despite its limitations, the developed system provides a basis for future TV pumppless perfusion systems. Its simplicity and scalability may support the development of more accessible and miniaturised OOC models.

References

[1] Dongeun Huh et al. "Reconstituting Organ-Level Lung Functions on a Chip". In: *Science* 328.5986 (June 2010), pp. 1662–1668. ISSN: 0036-8075. DOI: 10.1126/science.1188302.

[2] Chak Ming Leung et al. "A guide to the organ-on-a-chip". In: *Nat. Rev. Methods Primers* 2.33 (May 2022), pp. 1–29. ISSN: 2662-8449. DOI: 10.1038/s43586-022-00118-6.

[3] Alexandra Sontheimer-Phelps, Bryan A. Hassell, and Donald E. Ingber. "Modelling cancer in microfluidic human organs-on-chips". In: *Nat. Rev. Cancer* 19 (Feb. 2019), pp. 65–81. ISSN: 1474-1768. DOI: 10.1038/s41568-018-0104-6.

[4] Deepanmol Singh et al. "Journey of organ on a chip technology and its role in future healthcare scenario". In: *Applied Surface Science Advances* 9 (Apr. 2022), p. 100246. DOI: 10.1016/j.apsadv.2022.100246.

[5] Xiaoyan Liu, Wenfu Zheng, and Xingyu Jiang. "Cell-Based Assays on Microfluidics for Drug Screening". In: *ACS Sens.* 4.6 (June 2019), pp. 1465–1475. DOI: 10.1021/acssensors.9b00479.

[6] Seung-A. Lee et al. "Spheroid-based three-dimensional liver-on-a-chip to investigate hepatocyte–hepatic stellate cell interactions and flow effects". In: *Lab Chip* 13.18 (Aug. 2013), pp. 3529–3537. ISSN: 1473-0197. DOI: 10.1039/C3LC50197C.

[7] Y. Yuan et al. "Flow modulates coronary venular permeability by a nitric oxide-related mechanism". In: *American Journal of Physiology-Heart and Circulatory Physiology* (Aug. 1992). DOI: 10.1152/ajpheart.1992.263.2.H641.

[8] H. Jo et al. "Endothelial albumin permeability is shear dependent, time dependent, and reversible". In: *American Journal of Physiology-Heart and Circulatory Physiology* (June 1991). DOI: 10.1152/ajpheart.1991.260.6.H1992.

[9] Joohyung Lee et al. "A microfluidic cardiac flow profile generator for studying the effect of shear stress on valvular endothelial cells". In: *Lab Chip* 18.19 (Sept. 2018), pp. 2946–2954. ISSN: 1473-0197. DOI: 10.1039/C8LC00545A.

[10] Kattika Kaarj and Jeong-Yeol Yoon. "Methods of Delivering Mechanical Stimuli to Organ-on-a-Chip". In: *Micromachines* 10.10 (Oct. 2019), p. 700. ISSN: 2072-666X. DOI: 10.3390/mi10100700.

[11] Shashwat S. Agarwal et al. "A Modular, Cost-Effective, and Pumpless Perfusion Assembly for the Long-Term Culture of Engineered Microvessels". In: *Micromachines* 16.3 (Mar. 2025), p. 351. ISSN: 2072-666X. DOI: 10.3390/mi16030351.

[12] Feng Zhang et al. "Pump-Less Platform Enables Long-Term Recirculating Perfusion of 3D Printed Tubular Tissues". In: *Adv. Healthcare Mater.* 12.27 (Oct. 2023), p. 2300423. ISSN: 2192-2640. DOI: 10.1002/adhm.202300423.

[13] Feng Zhang et al. "Pump-Less Platform Enables Long-Term Recirculating Perfusion of 3D Printed Tubular Tissues". In: *Adv. Healthcare Mater.* 12.27 (Oct. 2023), p. 2300423. ISSN: 2192-2640. DOI: 10.1002/adhm.202300423.

[14] Agnes Purwidyantri and Briliant Adhi Prabowo. "Tesla Valve Microfluidics: The Rise of Forgotten Technology". In: *Chemosensors* 11.4 (Apr. 2023), p. 256. ISSN: 2227-9040. DOI: 10.3390/chemosensors11040256.

[15] Pengcheng Zhao et al. "A time sequential microfluid sensor with Tesla valve channels". In: *Nano Res.* 16.9 (Sept. 2023), pp. 11667–11673. ISSN: 1998-0000. DOI: 10.1007/s12274-023-5778-8.

[16] Huanhuan Shi et al. "Wearable tesla valve-based sweat collection device for sweat colorimetric analysis". In: *Talanta* 240 (Apr. 2022), p. 123208. ISSN: 0039-9140. DOI: 10.1016/j.talanta.2022.123208.

[17] Jie Gong et al. "Numerical Calculation of Gas–Liquid Two-Phase Flow in Tesla Valve". In: *Aerospace* 11.5 (May 2024), p. 409. ISSN: 2226-4310. DOI: 10.3390/aerospace11050409.

[18] P. F. Lalor and D. H. Adams. "Adhesion of lymphocytes to hepatic endothelium." In: *Mol. Pathol.* 52.4 (Aug. 1999), pp. 214–219. ISSN: 1366-8714. DOI: 10.1136/mp.52.4.214.

[19] Hassan Rashidi et al. "Fluid shear stress modulation of hepatocyte-like cell function". In: *Arch. Toxicol.* 90.7 (July 2016), pp. 1757–1761. ISSN: 1432-0738. DOI: 10.1007/s00204-016-1689-8.

[20] Sebastian Bohm et al. "Highly efficient passive Tesla valves for microfluidic applications". In: *Microsyst. Nanoeng.* 8.97 (Sept. 2022), pp. 1–12. ISSN: 2055-7434. DOI: 10.1038/s41378-022-00437-4.

[21] Piyush R. Porwal et al. "Heat transfer and fluid flow characteristics in multistaged Tesla valves". In: *Numerical Heat Transfer, Part A: Applications* (Mar. 2018). URL: https://www.tandfonline.com/doi/full/10.1080/10407782.2018.1447199#abstract.

[22] Sebastian Bohm et al. "Highly efficient passive Tesla valves for microfluidic applications". In: *Microsyst. Nanoeng.* 8.97 (Sept. 2022), pp. 1–12. ISSN: 2055-7434. DOI: 10.1038/s41378-022-00437-4.

[23] Ronald Louis Bardell. "The diodicity mechanism of tesla-type no-moving-parts valves". PhD thesis. University of Washington Seattle, WA, USA, 2000.

[24] Xinchen Zhang et al. "Study on the influence of different structural parameters on the performance of Tesla valve". In: *J. Phys. Conf. Ser.* 2707.1 (Feb. 2024), p. 012092. ISSN: 1742-6596. DOI: 10.1088/1742-6596/2707/1/012092.

[25] Adrian R. Gamboa, Christopher J. Morris, and Fred K. Forster. "Improvements in Fixed-Valve Micropump Performance Through Shape Optimization of Valves". In: *J. Fluids Eng.* 127.2 (Dec. 2004), pp. 339–346. ISSN: 0098-2202. DOI: 10.1115/1.1891151.

[26] Wenhui Liu et al. "Comparative analysis of performance of different types of Tesla valves". In: *J. Phys. Conf. Ser.* 2854.1 (Oct. 2024), p. 012103. ISSN: 1742-6596. DOI: 10.1088/1742-6596/2854/1/012103.

[27] Yunhao Bao and Huanguang Wang. "Numerical study on flow and heat transfer characteristics of a novel Tesla valve with improved evaluation method". In: *Int. J. Heat Mass Transfer* 187 (May 2022), p. 122540. ISSN: 0017-9310. DOI: 10.1016/j.ijheatmasstransfer.2022.122540.

[28] S. M. Thompson et al. "Numerical Investigation of Multistaged Tesla Valves". In: *J. Fluids Eng.* 136.8 (May 2014), p. 081102. ISSN: 0098-2202. DOI: 10.1115/1.4026620.

[29] Peilu Hu et al. "Numerical investigation of Tesla valves with a variable angle". In: *Phys. Fluids* 34.3 (Mar. 2022), p. 033603. ISSN: 1070-6631. DOI: 10.1063/5.0084194.

[30] Bastien Venzac et al. "PDMS Curing Inhibition on 3D-Printed Molds: Why? Also, How to Avoid It?" In: *Anal. Chem.* 93.19 (May 2021), pp. 7180–7187. ISSN: 0003-2700. DOI: 10.1021/acs.analchem.0c04944.

[31] Mees N. S. de Graaf et al. "Pressure-driven perfusion system to control, multiplex and recirculate cell culture medium for Organs-on-Chips". In: *bioRxiv* (July 2022), p. 2022.07.21.500785. DOI: 10.3390/mi13081359. eprint: 2022.07.21.500785.

[32] *FLOW UNIT - Bidirectional Microfluidic Flow Sensor - Fluigent*. [Online; accessed 2. Jul. 2025]. June 2025. URL: https://www.fluigent.com/research/instruments/sensors/flow-unit.

Appendix

During the preparation of this work, I used ChatGPT to improve grammar and text structure. I used ChatPDF to improve the text structure of the abstract. I used Cutout.pro to improve the image quality. After using these tools, I thoroughly reviewed and edited the content as needed, taking full responsibility for the final outcome.

Appendix A

This appendix describes the method used to measure the pressure drop across the VOC at specific applied flow rates. Prior to each test, the full VOC chip (consisting of the bonded PDMS VOC chip and glass slide) was exposed to a second plasma treatment in a plasma cleaner (henniker plasma, HPT-200), this time to make the channels hydrophilic rather than for bonding purposes. Subsequently, the full VOC chip was connected to two Push Pull controllers (Fluigent) to regulate the pressure difference in the setup, two fluid reservoirs, and one FLOW UNIT M+ sensor (Fluigent) to measure the flow rate through the setup, and a reverse flow was established through the VOC. The liquid used for the measurements was a solution of 0.33 % red food couloring in deionised water at 20 °C. Once the setup was assembled, any air bubbles present within the VOC were removed, and the weight of both reservoirs, each filled with the dyed water solution, were measured and equalised. The pressure difference was measured at the predefined flow rates of 5, 12.5, 25, 50, 100 and 150 μ l/min. After completing the reverse flow measurements, the full VOC chip was reconnected to establish a forward flow, and the same procedure was repeated. The VOC design was tested in triplicate (n = 3).